Proc. Of the 5th International E-Conference on Advances in Engineering, Technology and Management - ICETM 2021

ISBN: 978-1-63248-192-4 DOI: 10.15224/ 978-1-63248-192-4-13

Structural Behavior of Ferrocement Composite Light Weight Box Girder

[Yousry B.I. Shaheen, Zeinab A. Etman and Ahmed Badr EL-din]

***Abstract*— This paper presents a new box girder reinforced with various types of metallic and non-metallic mesh reinforcement materials. The main objective of the current research is to estimate the structural behaviour of thin ferrocement box bridges reinforced with composite material. Experimental investigation has been carried out on nine girders. The dimensions of the girder were 2000 mm length, 500 mm width and 350 mm thickness but with various layers numbers made from different mesh types. Cracking patterns, tensile and compressive strains, deformation characteristics, ductility ratio, and energy absorption properties were observed and measured at all stages of loadings. Experimental results were then compared to analytical models using (ABAQUS/Explicit) programs. The results showed that the type of reinforcement affects the ductility ratio, ultimate strength and energy absorption properties of the proposed girders. The study also revealed that the expanded metal mesh and welded steel mesh using in reinforcing the ferrocement girders are effective. Moreover, the developed ferrocement box girders have high ductility ratio, strength and energy absorption properties and are lighter in weight which are very useful for dynamic applications compared to the conventional RC girders, which could be useful for developed and developing countries alike. The Finite Element (FE) simulations achieved better results in comparison with the experimental results.**

***Keywords*: ferrocement; composite material; Expanded; Welded; Tenax; experimental; FE modeling; ABAQUS/Explicit.**

I. Introduction

Ferrocement material has been defined by the American Concrete Institute (ACI committee 549, 2009) as "A type of reinforced concrete commonly constructed of hydraulic cement mortar reinforced with closely spaced layers of relatively small wire diameter mesh. The mesh may be made of metallic or other suitable materials. The fineness of the mortar matrix and its composition should be compatible with the opening and tightness of the reinforcing system it is meant to encapsulate. The matrix may contain discontinuous fibers".

Yousry B.I. Shaheen (Professor)
Department of Civil Engineering, Faculty of Engineering, Menoufia University, Egypt,

Zeinab A. Etman (Professor)
Department of Civil Engineering, Higher Institute of Engineering and Technology, Menoufia
Egypt

Ahmed Badr El-din (Ph.D student)
Department of Civil Engineering, Higher Institute of Engineering and Technology, Kafr El-sheikh
Egypt,

Shaheen and Eltahawy (2017) presents a new precast U-shape ferrocement forms reinforced with various types of metallic and non-metallic mesh reinforcement. The experimental program comprised casting and testing ten slabs having the total dimensions of 500x100x2500 mm incorporating 40 mm thick U shape permanent ferrocement forms. The experimental results show that results showed that high ultimate and serviceability loads, better crack resistance control, high ductility, and good energy absorption properties could be achieved by using the proposed slabs and low cost compared with control specimen.

In the same vein, Abdul-Fataha (2014), Shaheen et al. (2014) employed numerical models and designed an experimental program to investigate the structural behavior of twelve ferrocement beams under three point loadings up to failure. The twelve beams were different in terms of the types of reinforcement: steel bars, traditional wire meshes, and welded and expanded wire meshes. The results of the numerical models and experimental tests indicated that the beam with fiberglass meshes gives the lowest first crack load and the maximum load. Their results concluded further that the ferrocement beam reinforced with four layers of welded wire meshes had better structural behavior than those beams reinforced with other types of wire meshes.

The effect of the strength of ferrocement jackets for initially damaged exterior RC beam-column joints is presented by (Singh, Bansal et al. 2015). In this study, the experimental observation noticed an improvement in the ultimate load, yield load carrying capacity with increase in stiffness of the ferrocement-jacketed joints in comparison with the control joint.

Ramakrishnan et al. (2020) studied the strength and flexural behavior of ferrocement box beams for precast purposes. By partially replacing the cement (binder) with various percentages of Silica Fume (SF) (0–25% in steps of 5%), ferrocement box beam is cast to ascertain whether there is an increase or decrease in compressive and tensile strength due to the addition of SF.

From the results of compressive and split tensile strengths, it is found that 10% of SF replacement produced higher strength. After obtaining the optimum percentage of micro filler, two ferrocement box beams with SF (10% SF with 90% cement) and two without SF and two ferrocement solid beams are cast and tested for bending, under two-point loading with two layers of wire mesh. The flexural strength of ferrocement box beam without micro filler is compared with ferrocement solid beam. The test results indicated that the flexural strength drop for the beam with voids is less in comparison with a solid beam due to the reduction in self-weight of the hollow box beam.

ISBN: 978-1-63248-192-4 DOI: 10.15224/ 978-1-63248-192-4-13

Furthermore, many attempts have been made to improve the practical use of the ferrocement I-beams by developing its ductile behavior. For example, the evaluation of the actual flexural capacity of the ferrocement I-beam with additional layers of wire mesh in the flange section as compared to the theoretical analysis computation is illustrated by (Acma, Dumpasan et al. 2015). The design and construction of the ferrocement channels were presented with various materials (e.g., meshes and mortar). In addition, an optimal combination of meshes was obtained and finite element FE models of the channels were implemented using ABAQUS Unified FEA (Eskandari and Madadi 2015).

Dajun (1993) used the ferrocement technique for the construction of bridges in China. Examples of such applications include: two-way curved shallow shells, thin-walled slabs for box beams, stiffeners for box bridges in long-span suspension bridges, floating thin- walled caissons for bridge piers, and protective tubes for palls.

Abbas et al. (2020) studied the flexural response of hollow high strength concrete beams considering different size reductions. 14 reinforced concrete solid and hollow beams were tested under four-point bending test to evaluate the flexural behavior of hollow concrete beams. The experimental program focused on two main variables: the size reduction percentage and the inclusion of steel fiber. Ten hollow beams with central square holes with side lengths of 60, 80, and 100mm in addition to four solid beams were fabricated to evaluate the test parameters. These beams were either reinforced with 1% steel fiber or contained no fiber at all.

In addition to the experimental work, analytical formulas were introduced to evaluate the cracking and peak loads of the hollow beams. The test results showed that ductility of hollow beams with size reductions of 16% and 28.4% was higher than that of the reference solid beam, while the ductility of the hollow beam with 44.4% size reduction was quite comparable to that of the solid beam. Moreover, the toughness values of the hollow beams were higher by 19 to 37% than that of the reference solid beam. Based on the obtained results, it can be concluded that hollow reinforced concrete beams with 1.0% steel fiber and with size reduction up to 44.4% can replace solid beams without suffering significant reductions in strength, ductility and toughness.

Yang et al. (2021) investigated a new mechanical model of polyvinyl alcohol fiber–reinforced ferrocement cementatious composite (PVA-RFCC), which was reinforced with both PVA fiber and steel wire mesh (SWM). A series of experiments were conducted to study their mechanical properties, and a comparative analysis was also performed to evaluate their flexural toughness.

The experimental results showed that the flexural properties of the PVA-RFCC specimens can be markedly improved compared with PVA-ECC (PVA-engineered cementitious composites) specimens. The highest increments in the initial stiffness, cracking strength, displacement ductility coefficient, and toughness of the PVA-RFCC specimens were improved by 62.4%, 174.7%, 251.0%, and 192.5%, respectively.

Naser et al. (2020) applied an experimental investigation to study the effect of using different types of reinforcement on the flexural behavior of ferrocement thin hollow core slabs with embedded PVC pipes. Twelve slabs of 1100 × 400 × 55 mm dimensions were casted and tested till failure. The effect of four different types of reinforcement was investigated in this study including; steel wire mesh, macro and micro steel fibers or a combination of both, steel bars and CFRP bars.

The results showed that the slab reinforced with only macro steel fibers provided the highest flexural strength, while that reinforced with steel bars showed the highest stiffness and lowest deflection among all tested slabs. Also, the dry design density for all the hollow core slabs was determined to be below 2000 kg/m3 which is within the requirements of light weight concrete as set by most codes of practice.

The main objective of this paper is to study the structural behavior of ferrocement box girders reinforced with different types of meshes. These types are welded, expanded and Tenax mesh. Moreover, the current study aims to compare the behavior of ferrocement girders with the behavior of congenitally reinforced concrete girders reinforced with ordinary mild steel bars only. It seeks to simulate the tested girders by using finite element ABAQUS program to investigate their structural behavior up to failure.

II. Experimental program

The experimental program includes the construction and testing of nine box girder 2000 mm long, 500 mm wide and 350 mm total thickness. The main goal is to investigate the ultimate load, flexural behaviour, ductility ratio, energy absorption and mode of failure at collapse of the control box girders, which are reinforced with steel bars and steel stirrups and, then, to compare their behaviour with those ferrocement box bridges reinforced with welded galvanized steel mesh and expanded metal mesh and Tenax mesh. Skeletal steel bars and steel stirrups are used with steel and Tenax meshes. Four designations series are then developed as shown in Table **I**, along with the details of the experimental program of all the test specimens. Fig.1 also reveals all the details of reinforcement for all specimens.

Proc. Of the 5th International E-Conference on Advances in Engineering, Technology and Management - ICETM 2021

ISBN: 978-1-63248-192-4 DOI: 10.15224/ 978-1-63248-192-4-13

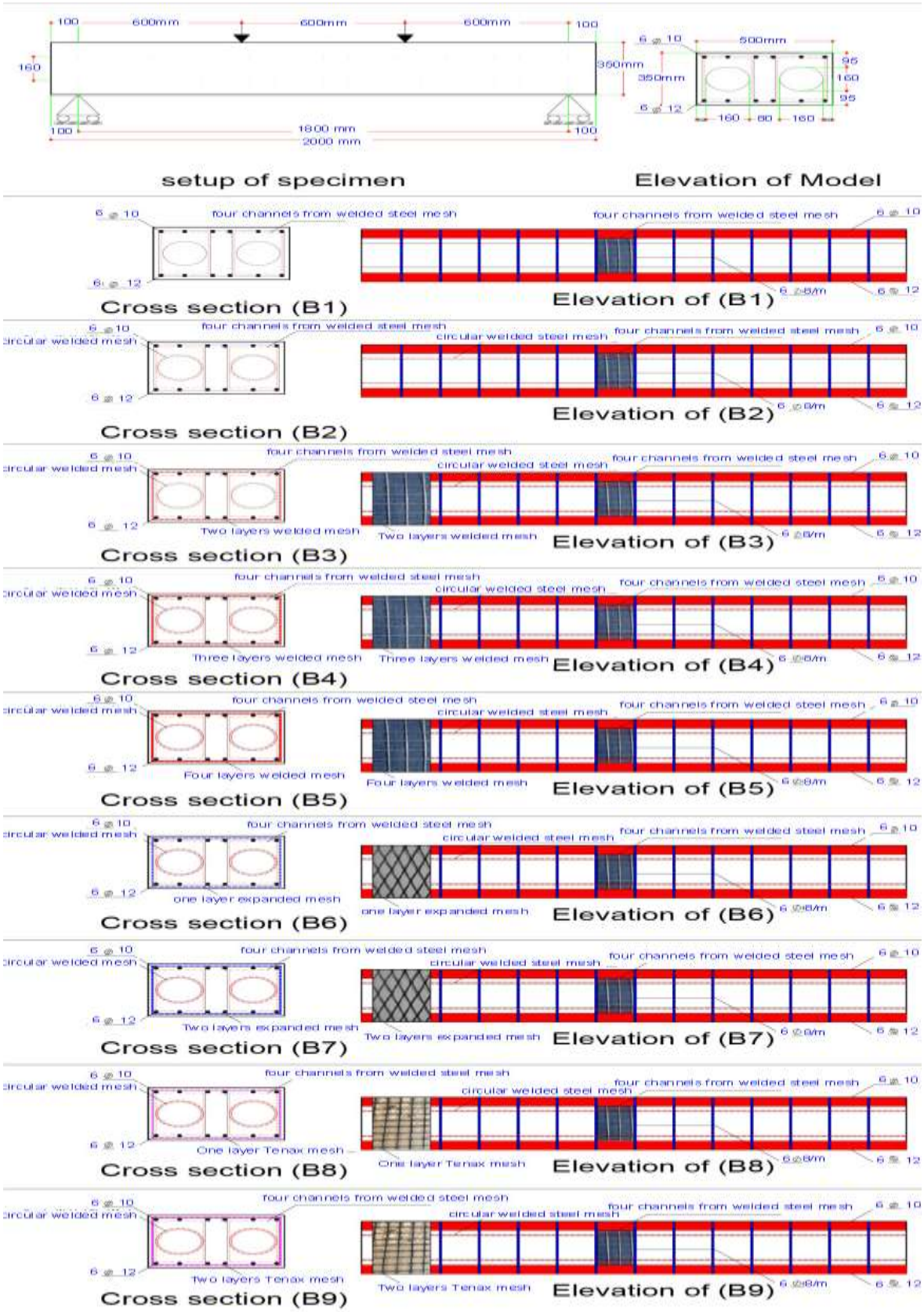

Figure 1. Reinforcement details of the tested specimen

Proc. Of the 5th International E-Conference on Advances in Engineering, Technology and Management - ICETM 2021

ISBN: 978-1-63248-192-4 DOI: 10.15224/ 978-1-63248-192-4-13

TABLE I. DETAILS OF EXPERIMENTAL PROGRAM

Specimens designation	Code of girder	Reinforcement wire mesh	Reinforcing steel bars and stirrups		
			Tens.	Comp.	Stirrups
1	B1	Conventional	6 Φ 12	6 Φ 10	6 Φ8/m
	B2	Conventional + one layer of welded steel mesh as a circle around openings.	6 Φ 12	6 Φ 10	6 Φ8/m
2	B3	Two layers of welded steel mesh at each side + two layers of welded steel mesh as a circle around openings.	6 Φ 12	6 Φ 10	6 Φ8/m
	B4	Three layers of welded steel mesh at each side + two layers of welded steel mesh as a circle around openings.	6 Φ 12	6 Φ 10	6 Φ8/m
	B5	Four layers of welded steel mesh at each side + two layers of welded steel mesh as a circle around openings.	6 Φ 12	6 Φ 10	6Φ8//m
3	B6	one layer of expanded steel mesh at each side + two layers of welded steel mesh as a circle around openings.	6 Φ 12	6 Φ 10	6 Φ8/m
	B7	Two layers of expanded steel mesh at each side + two layers of welded steel mesh as a circle around openings.	6 Φ 12	6 Φ 10	6 Φ8/m
4	B8	one layer of Tenax mesh at each side + two layers of welded steel mesh as a circle around openings.	6 Φ 12	6 Φ 10	6 Φ8/m
	B9	Two layers of Tenax mesh at each side + two layers of welded steel mesh as a circle around openings.	6 Φ12	6 Φ 10	6 Φ8/m

A. *Materials*

The fine aggregate used in the experimental program was of natural siliceous sand. Its characteristics satisfy the specification E.S.S. 1109/2008 . It was clean and nearly free from impurities with a specific gravity 2.6 t/m3 and a modulus of fineness 2.7. The coarse aggregate used was crushed dolomite, which satisfied the requirements of the E.S.S. 1109/2008 with a specific gravity of 2.75 t/ m3 and a crushing modulus of 18.5% absorption of 2.1%. The shape of these particles was irregular and angular with a relatively high percentage of elongated particles and a very low percentage of flat particles. The cement used was the Ordinary Portland cement, type produced by the Suez cement factory. Its chemical and physical characteristics satisfied the Egyptian Standard Specification E.S.S.4756-11 (2012).Silica fume (S.F) was employed in the present work to enhance the strength of ferrocement mortar and concrete core. It was used as partial replacement by weight of cement in the mortar mixtures. The S.F. had an average particle size of 0.1 micrometer and a silicon dioxide content of 93%. Fly ash was used as ratio of cement. It complies with the chemical and physical requirements of ASTM C618 and relevant international quality standards for fly ash. Fly ash had a relatively low specific gravity and Blaine fineness of 2.10 and 330kg /m2, respectively. Water used was the clean drinking fresh water free from impurities used for mixing and curing the R.C. beams tested according to the E.C.P. 203/2007. Super plasticizer used was a high rang water reducer HRWR. It was used to improve the workability of the mix. The admixture used was produced by CMB GROUP under the commercial name of Addicrete BVF. It meets the requirements of ASTM C494 (type A and F) . The admixture is a brown liquid having a density of 1.18 kg/liter at room temperature. The amount of HRWR was 1.0% of the cement weight. Polypropylene fibers e300 was used. It was available in the Egyptian markets. It was used in concrete mixes to produce fibrous concrete jacket to improve the concrete characteristics. It complies with ASTM C1116 (2015) The percentage of addition was chosen as 900 Gm/m^3 based on the recommendations of manufacture. The technical specifications and mechanical properties of Polypropylene fibers e300 as provided by producing company are given in Table II.

TABLE II. CHEMICAL AND PHYSICAL PROPERTIES OF FIBER MESH E300 [15].

Absorption	Nil
Specific Gravity	0.91
Fiber Length	Single cut lengths
Electrical Conductivity	Low
Acid & Salt Resistance	High
Melt Point	324°F (162°C)
Thermal Conductivity	Low
Ignition Point	1100°F (593°C)
Alkali Resistance	Alkali Proof

Proc. Of the 5th International E-Conference on Advances in Engineering, Technology and Management - ICETM 2021

ISBN: 978-1-63248-192-4 DOI: 10.15224/ 978-1-63248-192-4-13

Reinforcing steel; High tensile deformed steel bars of 12 mm diameter in the tension side and high tensile steel bars of 10 mm diameter in the compression side which its proof stress and ultimate strength of the steel material were 551N/mm² and 670 N/mm² were used to reinforce the reinforced concrete and Ferrocement box bridges of the test. Expanded steel mesh is used as reinforcement for ferrocement girders. The technical specifications and mechanical properties of expanded metal mesh as provided by producing company are given in Table III and shown in Fig.2.

TABLE III .TECHNICAL AND MECHANICAL PROPERTIES OF EXPANDED METAL MESH [1]

Style	1532
Sheet Size	1 m × 10
Weight	1.3 Kg/m2
Diamond size	16 × 31mm
Dimensions of strand	1.25 × 1.5mm
Proof Stress (N/mm2)	199
Proof Strain × 10-3	9.7
Ultimate Strength (N/mm2)	320
Ultimate Strain× 10-3	59.2

The Welded steel mesh used was obtained from China, and it was used as reinforcement for ferrocement girders. The technical specifications and mechanical properties of welded steel mesh as provided by producing company are given in Table IV. It is comply with of ACI 549.1R-97 (2009).

TABLE IV.TECHNICAL AND MECHANICAL PROPERTIES OF WELDED METAL MESH[1]

Dimensions	12.5mm × 12.5 mm
Weight	430 gm /m^2
Proof Stress	737 N/mm^2
Ultimate Strength (N/mm^2)	834 N/mm^2
Ultimate Strain × 10^{-3}	58.8
Proof Strain × 10^{-3}	1.17

TENAX LBO SAMP (330) is polypropylene Geogrid especially for reinforcement applications. The Geogrid is manufactured from a unique process of extrusion and biaxial orientation to enhance their tensile properties It features consistently high tensile strength and modulus, excellent resistance to construction damages and environmental exposure. Properties of this mesh can be shown in Table V.

TABLE V. PHYSICAL CHARACTERISTIC OF TENAX (LBO 330) FROM ITS DATA SHEET.

Structure	Biaxial geogrid
Mesh type	Rectangular apertures
Standard color	Black
Polymer type	Polypropylene
Carbon black content	2%
Dimensional characteristics	(LBO 330) Samp
Aperture size Md	40 mm
Aperture size Md	27 mm
Mass per unit area	420 g/m2
Roll width	4 m
Roll length	50 m
Roll diameter	.52 m
Roll volume	1.1 m3
Gross roll weight	137 kg

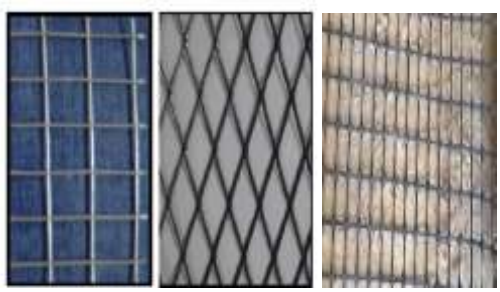

Welded steel mesh | Expanded steel mesh | Tenax mesh (LBO330)

Figure 2. Types of meshes used in experimental program

B. Concrete mix

The main purpose of mix design was to determine how the high amount of cement could be partially replaced by silica fume and fly ash to increase strength of mortar matrix with no detrimental effects on the quality and properties of the mix in both the fresh and hardened states. The requirement of good workability was essential, to allow the mortar matrix to penetrate through the layers of steel mesh reinforcement. A super plasticizing agent was used to increase flow characteristics and accelerate the early strength development. Mortar mixtures for the ferrocement were made using a water to cement ratio of 0.35, dolomite to sand ratio of 2:1 and super-plasticizer of 2% by weight of cement, while 10% by weight of cement was replaced by S.F and 20% by weight of cement was replaced by fly ash and the percentage of addition of fiber was chosen as 900 gm/m^3. The density of the mortar mix was approximately 2200 kg/m^3. The average compressive strength after 28 days was 40 MPa.

Preparation of test specimens

The mold from rectangular forms from contras wood with entire size of 500x350x2000 mm was prepared and used for casting beams. The pipes from plastic with diameter 160 mm and 220cm length were prepared and used to keep the required voids. . The ferrocement forms were left for 24 hours in the mold before disassembling the mold. Lastly, the forms were covered with wet burlap for 28 days. All of previous steps are shown in Fig. (3).

D. Test setup

After 28 days, the specimens were painted with white paints to facilitate the crack detection during the testing process. The specimens were tested on a testing loading frame with a four loading points. The span length was 1800 mm while the distance between the two loading points was 600 mm. linear variable differential transducers (LVDTs) were used to measure displacement at mid span and under points of loading while strain gauges attached to the top and bottom of the surface of concrete at the critical sections to evaluate its behavior. All the values of deflection at the variable positions and top and bottom strain values were recorded each 2 seconds computerized and save it as excel sheet . Test setup of specimen can be shown in Fig. (4).

Proc. Of the 5th International E-Conference on Advances in Engineering, Technology and Management - ICETM 2021

ISBN: 978-1-63248-192-4 DOI: 10.15224/ 978-1-63248-192-4-13

Figure 3. Steps of specimen preparation.

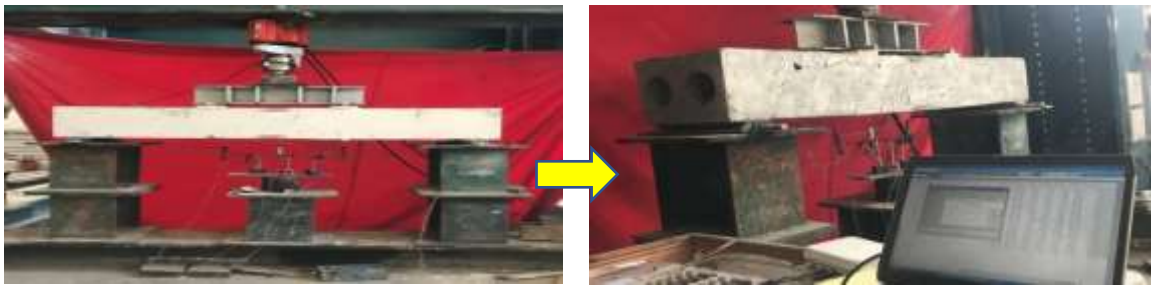

Figure 4. Test setup.

Proc. Of the 5th International E-Conference on Advances in Engineering, Technology and Management - ICETM 2021

ISBN: 978-1-63248-192-4 DOI: 10.15224/ 978-1-63248-192-4-13

E. *Experimental Results*

This section presents the experimental results of the test program and the discussion of the most important results. The results of the different test groups are compared to examine the effect of parameters on the structural responses of the proposed girders in terms of failure load, mode of failure, first crack load, service load, ductility ratio, and energy absorption were studied extensively. Table VI presents: first crack, serviceability, ultimate loads, ductility ratio and the energy absorption properties of all the tested girders.

Flexural Serviceability Load

The flexural serviceability load was calculated from the load-deflection curves. It is defined as the load corresponding to deflection equal to the span of the girder (1800 mm) divided by (constant=250) according to The Egyptian Code. Fig. (5) represents the values for the first cracking load, serviceability load and ultimate load for all the tested slabs. Maximum ultimate load reached (542.56) KN for B7 and minimum ultimate load achieved (420) KN. The main aim of calculating serviceability load is to evaluate the effect of using different meshes.

Ductility Ratio

The ductility ratio was calculated as the mid span deflection at the ultimate load to that of the first cracking load. Girders reinforced with expanded metal mesh and welded steel meshes were given higher ductility ratio than control beam. Girders B6 and B7 were given lower ductility ratio than control Girders. Fig. (6) shows ductility ratios for all tested girders.

Energy Absorption

The value of energy absorption was obtained by calculating the area under the load-deflection curve for each girder. Girders reinforced with expanded steel mesh were achieved higher energy absorption than control girders. Girders reinforced with welded metal mesh reached higher energy absorption than control girder. Fig. (7) emphasizes energy absorption for all tested girders. Higher ductility and energy absorption properties are very useful for dynamic applications.

TABLE VI. TEST RESULTS FOR ALL EXPERIMENTAL TEST SPECIMENS

Specimens Designation	Specimen No.	First Crack load (KN)	Serviceability Load (KN)	Ultimate Load (KN)	First Crack Deflection (mm)	Maximum deflection (mm)	Ductility Ratio	Energy Absorption (kN.mm)
1	**B1**	156.3	288	480	4.1	41	10	15390
	B2	165.6	370	480.7	3	51.9	17.3	21800
2	**B3**	160.5	370	523.6	2.67	25.78	9.6	9680
	B4	162.3	405	525	2.75	21.23	7.71	8250
	B5	165.3	322	531.1	1.2	19.355	16.1	6970
3	**B6**	157.5	455	522	2.1	16.58	7.89	13530
	B7	167.3	521	542.5	1.6	10.94	6.83	9880
4	**B8**	158.5	233	420.7	3.2	32.3	10.09	8930
	B9	160.3	403	482	2.1	43.03	20.5	7889

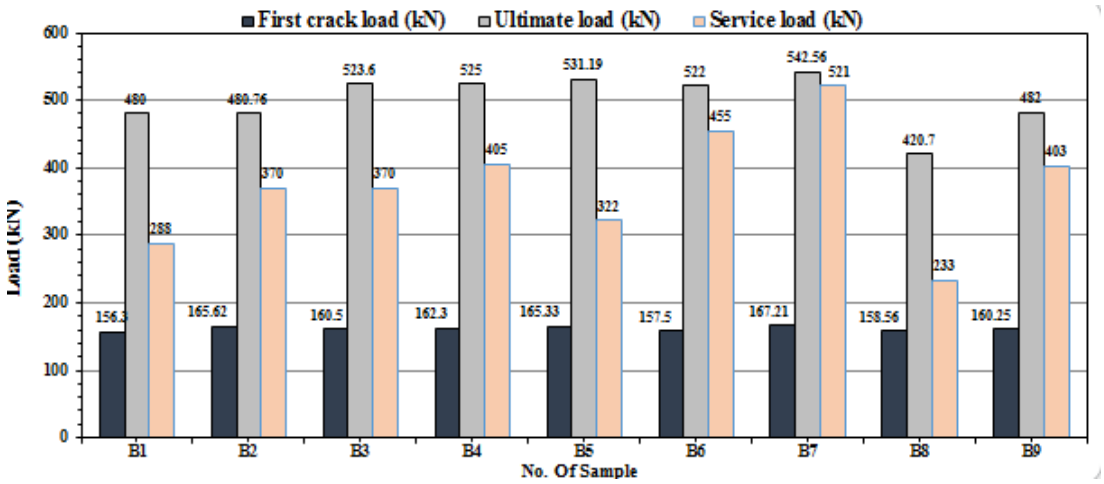

Figure 5. First crack, serviceability and ultimate loads of all tested girders.

Proc. Of the 5th International E-Conference on Advances in Engineering, Technology and Management - ICETM 2021

ISBN: 978-1-63248-192-4 DOI: 10.15224/ 978-1-63248-192-4-13

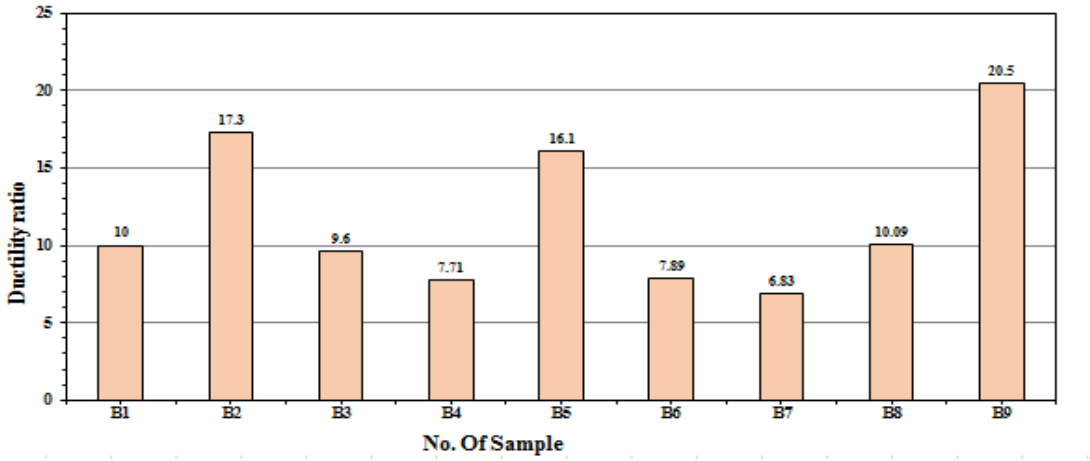

Figure 6. Ductility Ratio of all tested girders.

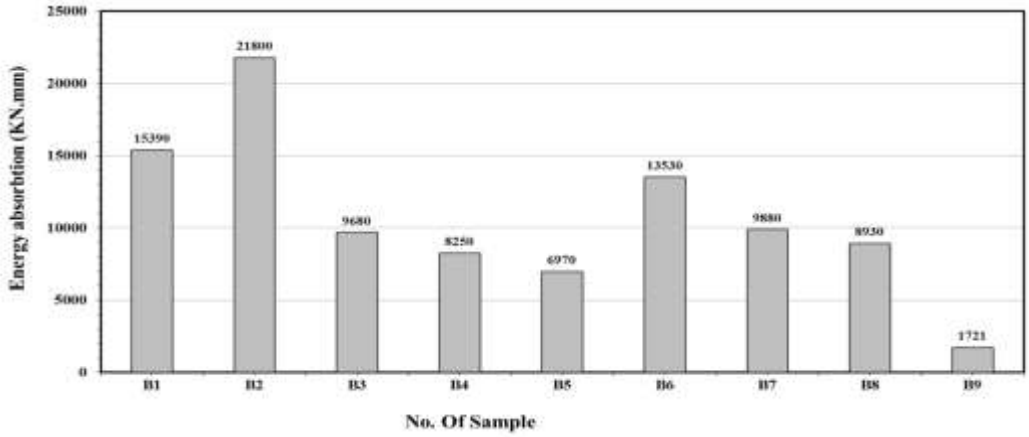

Figure 7. Energy absorption for all tested girders.

Load-Deflection Relationship

The load-deflection curves of the control specimen (B1) and (B2), the specimens incorporating ferrocement forms and reinforced with welded steel mesh in addition to steel bars (B3), (B4) and (B5), reinforced expanded steel mesh in addition to steel bars (B6) and (B7) and those reinforced with Tenax mesh (B8) and (B9). Figures (8-11) show load deflection curves for all the test specimens while Fig. (12) emphasizes comparison of load deflection curves for all the tested girders.

The load-deflection relationship for the control specimens was linear up to a load of 300-370 KN, approximately after which the relation became non-linear. For this group of specimens, the transition from the second to the third stages, as explained before, was not distinct as shown in Fig. (8). At failure, the mid-span deflection reached 41 mm, and 51 mm for specimens B1 and, B2 respectively. And the ultimate load was 480 and 481 KN for B1 and, B2, respectively.

For group 2 (designations B3,B4 and B5) specimens reinforced with two, three and four layers of welded steel mesh respectively., The load-deflection relationship was almost linear up to load of about 350,400 and 250 KN for specimens B3 , B4 and B5 respectively when the deviation from the linear relation started. Maximum deflection reached 25.78 mm, 21.21mm and 19.35 mm for specimens B3, B4 and B5 respectively as shown in Fig. (9).

For group 3, when B6 and B7 specimens reinforced with single and double layers of expanded steel mesh ,respectively. The load-deflection relationship was almost linear up to load of about 450 KN and 510 KN for specimens B6andB7 respectively when the deviation from the linear relation started as shown in Fig. (10).

At failure, the deflection reached 16.58 mm, 10.94 mm. For group 4 (designations B8 and B9) specimens reinforced with one and two layers of Tenax mesh respectively, the load-deflection relationship was almost linear up to load of about 250 kN and 400 KN when the deviation from the linear relation started as shown in Fig. (11). At failure, the deflection reached 32.3 mm and 43.03 mm for slabs B8 and B9, respectively.

Proc. Of the 5th International E-Conference on Advances in Engineering, Technology and Management - ICETM 2021

ISBN: 978-1-63248-192-4 DOI: 10.15224/ 978-1-63248-192-4-13

The Effect of Using Various Types of Meshes

In order to evaluate the effect of the reinforcing steel mesh type, it is compared to the results of groups reinforced with expanded wire mesh with that reinforced with welded steel mesh and tenax mesh. The scope of the comparison included the following girders: B3 was reinforced with double layers of welded wire mesh, B7 was reinforced with double layers of expanded steel mesh and B9 was reinforced with double layers of tenax mesh.

The best behaviour recorded was that of girder B7 that achieved higher first crack load, ultimate load and serviceability load with respect to steel bars and the number of steel mesh. The behaviour of first crack load, ultimate load and serviceability load of girder B3 was better than of girder B3. Fig. (13) show that relation between load and deflection for the compared girders.

Using double layers of expanded steel mesh as additional reinforcement increase the ultimate load by 3.6% , increase service load by 40% and decrease maximum mid-point deflection by 60% from that reinforced with double layers of welded steel mesh. While ssing double layers of welded steel mesh as additional reinforcement increases the ultimate load by 8.6 %, the service load by 1%, it decreases maximum mid-point deflection by 40 % from that reinforced with double layers of tenax mesh.

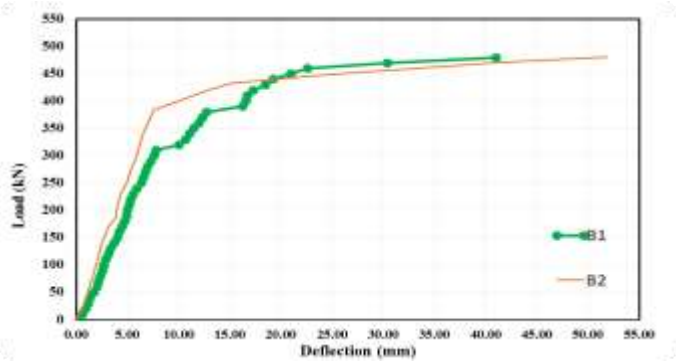

Figure 8. Load- deflection curves for group (1).

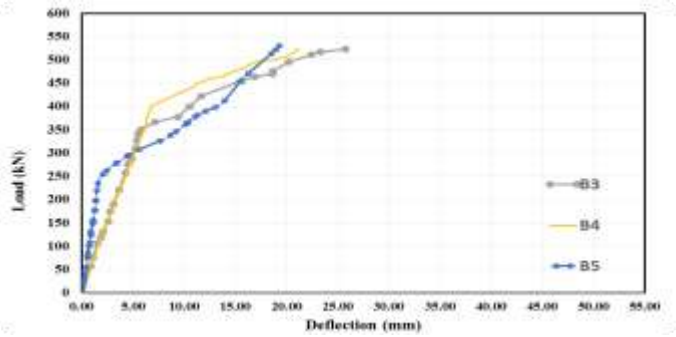

Figure 9. load- deflection curves for group (2).

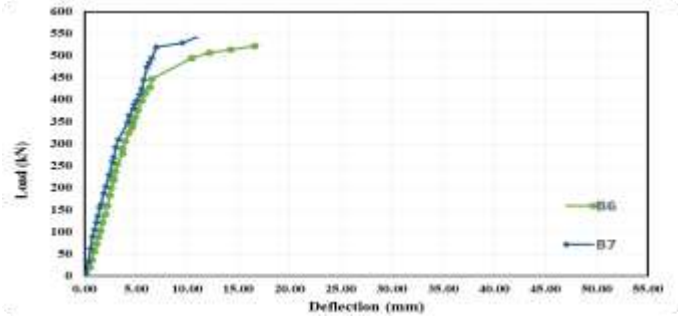

Figure 11. load- deflection curves for group (4).

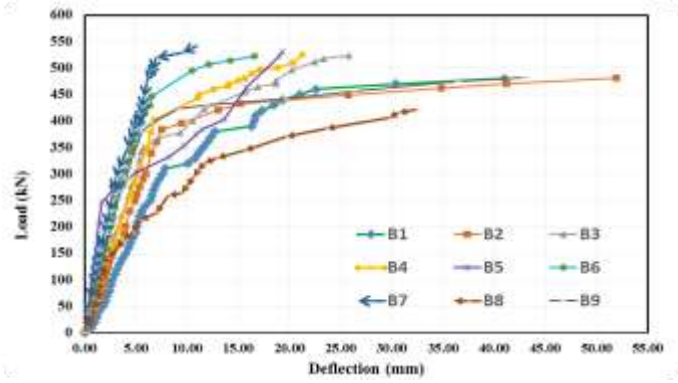

Figure 12. load- deflection curves for all tested girders.

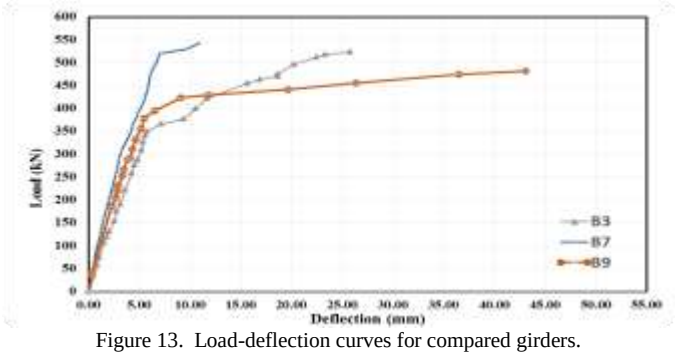

Figure 13. Load-deflection curves for compared girders.

Compressive and Tensile Strain

In Fig. (14) shows load strain curves for Control group specimens (B1 and B2). For girder B1 the compressive strain increased with the increase of the applied load. The maximum compressive strain reached about -0.000258 at maximum load 480 kN. However, the max tensile strain was 0.0345 at the same load. The maximum compressive strain at girder B2 reached about -0.00067at maximum load 481 kN. However, the max tensile strain was 0.03689 at the same load.

The load – compressive and tensile strain curves for group 2 (girders B3, B4 and B5) are plotted in Fig. (15). The curves show that the compressive strain increased with the increase of the applied load. At girder B3 the maximum compressive strain reached about -0.000604 at maximum load 523.6 KN. However, the max tensile strain was 0.00432 at the same load.

Proc. Of the 5th International E-Conference on Advances in Engineering, Technology and Management - ICETM 2021

ISBN: 978-1-63248-192-4 DOI: 10.15224/ 978-1-63248-192-4-13

For girder (B4) the maximum compressive strain reached about -0.00069 at maximum load 525 KN. However, the max tensile strain was 0.0204 at the same load. The maximum compressive strain reached about -0.00076 for girder (B5) at its failure load 531.19 KN. However, the max tensile strain was 0.0176 at this load.

For group 3 (specimens B6 and B7). The compressive strain increased with the increase of the applied load. For girder (B6) the maximum compressive strain reached about -0.000432 at maximum load 522 kN. However, the max tensile strain was 0.0068 at the same load. The maximum compressive strain at girder B7 reached about -0.000858 at maximum load 542.5 kN. However, the max tensile strain was 0.00527 at the same load as shown in Fig. (16).

For the last group specimens 4 (specimens B8 and B9). Fig. (17) show that the compressive strain increased with the increase of the applied load. For girder (B8) the maximum compressive strain reached about -0.00049 at maximum load 420.7 kN. However, the max tensile strain was 0.02313 at the same load. The maximum compressive strain at girder B9 reached about -0.00145at maximum load 482 kN. However, the max tensile strain was 0.033 at the same load.

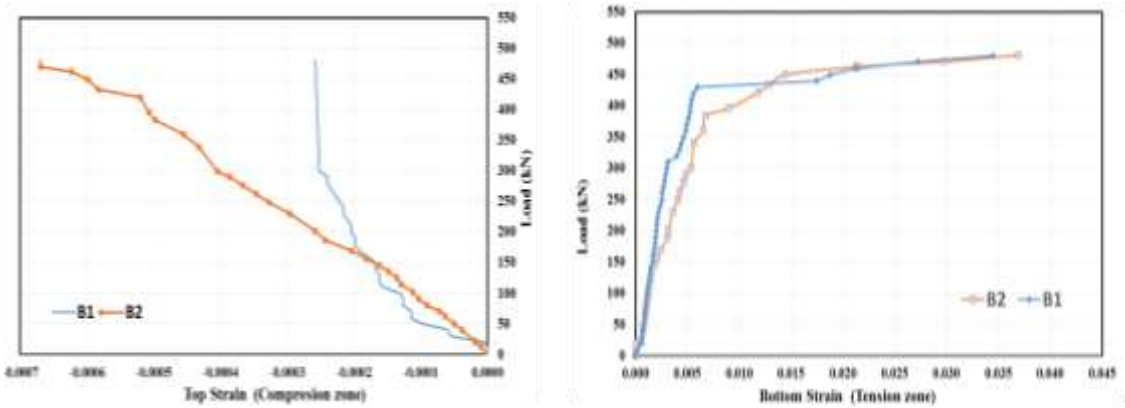

Figure 14. load- Compressive and tensile strain curves for group (1)

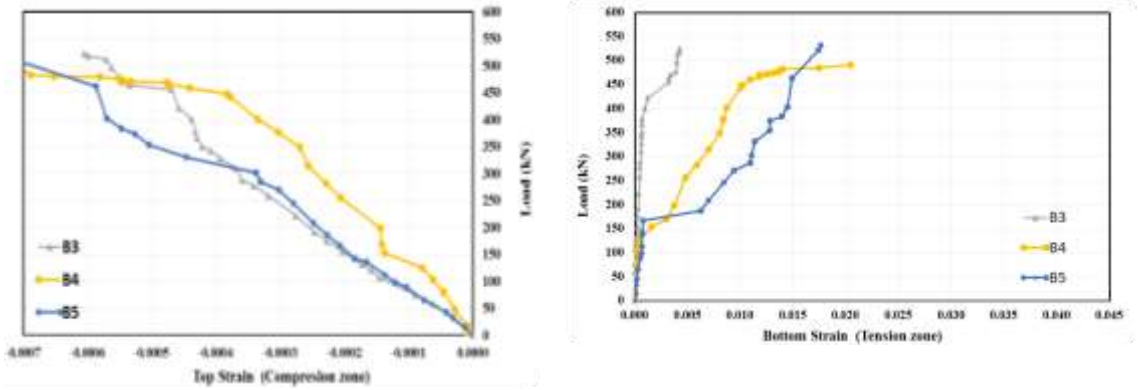

Figure 15. load- Compressive and tensile strain curves for group (2)

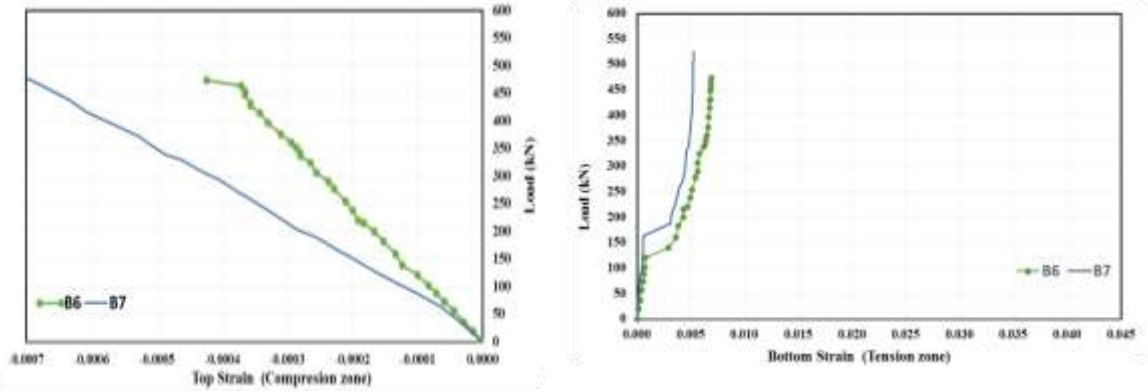

Figure 16. load- Compressive and tensile strain curves for group (3)

Proc. Of the 5th International E-Conference on Advances in Engineering, Technology and Management - ICETM 2021

ISBN: 978-1-63248-192-4 DOI: 10.15224/ 978-1-63248-192-4-13

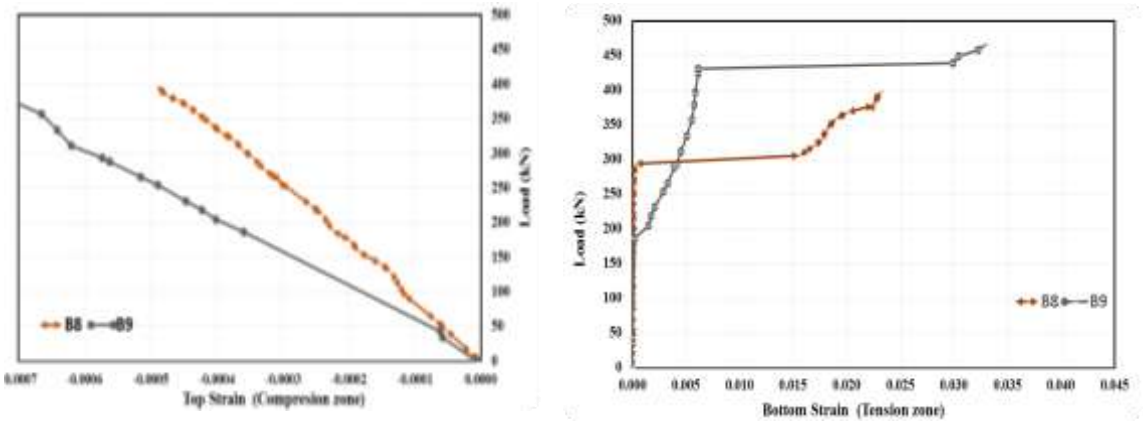

Figure 17. load- Compressive and tensile strain curves for group (4)

Cracking Patterns and Mode of Failure

Cracks were traced and marked throughout the side of the specimen. The first crack-load of each specimen, crack propagation, and failure mode were recorded. Flexural cracks developed near the mid-span of the. With the increase of the load, the cracks propagated vertically and new flexural cracks were developed rapidly. The cracks started to propagate wider when the specimens approached their failure load. The crack width was measured for all tested girders. It was observed that the cracks were very wide as a result of employing steel bars. It is interesting to note also that vertical flexural cracks started to develop close to the center of the span. As the load increased, more cracks started to develop and the crack at mid-span started to propagate vertically towards the top surface of the specimen, while most of the developed cracks did not continue propagating.

This could be attributed to the effect of steel mesh in controlling the crack width. For series designation (2, 3) which was reinforced with steel meshes combined with skeletal steel bars, the flexural cracks were less than series 1. At failure of girder B7, which was reinforced with two layers of expanded steel mesh and combined with steel bars, very narrow cracks were observed. For girders (B3, B4, B5 and B6) , it is can be noted that very fine vertical cracks were more developed than the previous designations and the cracks were uniformly distributed along the middle 2/3 of the span. The cracks for all tested girders can be shown in Fig. (18).

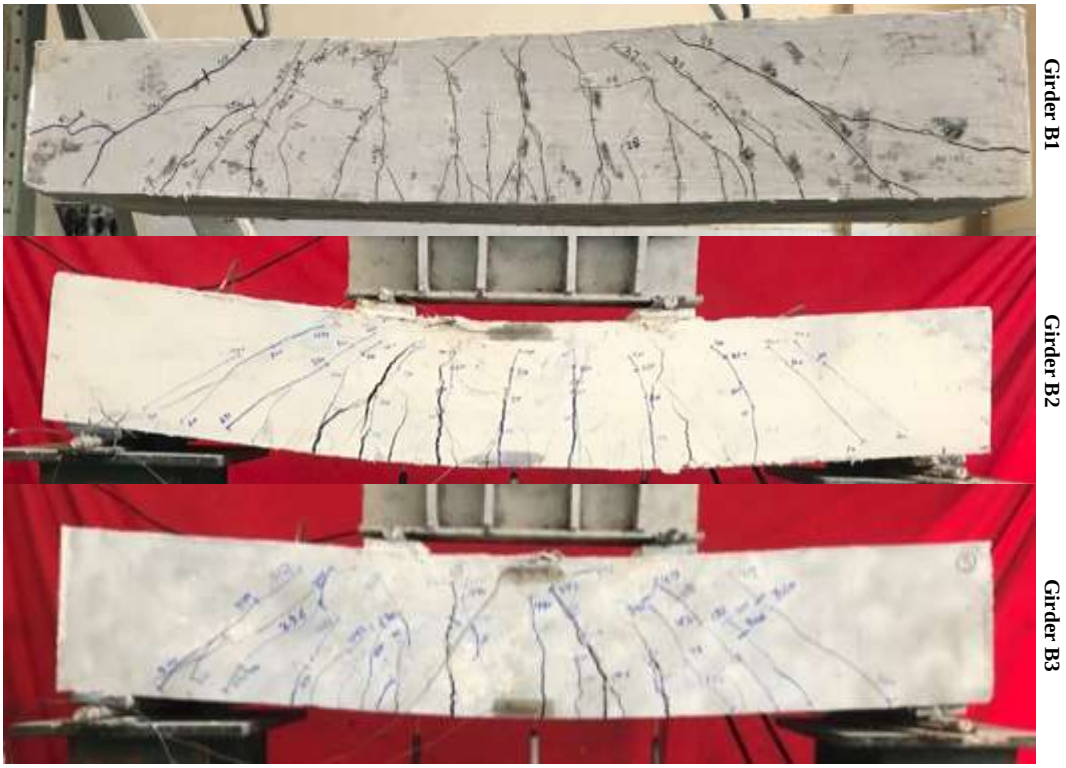

Figure 18. Cracking patterns for all tested girders.

ISBN: 978-1-63248-192-4 DOI: 10.15224/ 978-1-63248-192-4-13

Figure 18. (continued) Cracking patterns for all tested girders.

Proc. Of the 5th International E-Conference on Advances in Engineering, Technology and Management - ICETM 2021

ISBN: 978-1-63248-192-4 DOI: 10.15224/ 978-1-63248-192-4-13

III. Finite element simulation

The specimens of study were modeled as 3D structures in Abaqus. Concrete parts were modeled using C3D8R. Steel bars, welded and expanded steel mesh were modeled using T3D2 elements. Tenax mesh was modeled as shell element. Fig. (19) shows modeling of all parts (reinforced concrete box girder, Steel bars, four channels, circular welded mesh, welded, expanded metal mesh, tenax mesh) in Abaqus.

A. *Materials modeling*

Concrete material was modeled using Abaqus concrete damage plasticity model. This model uses the concept of isotropic damage elasticity in combination with isotropic compression and tensile plasticity to model the inelastic behavior of concrete. Tables VII and VIII present concrete elastic properties and concrete damaged plasticity model parameter used in analysis.

Steel reinforcement has approximately linear elastic behavior when the steel stiffness introduced by the Young's or elastic modulus keeps constant at low strain magnitudes. At higher strain magnitudes, it begins to have nonlinear, inelastic behavior, which is referred to as plasticity. The plastic behavior of steel is described by its yield point and its post-yield hardening. The shift from elastic to plastic behavior occurs at a yield point on a material stress-strain curve. Table IX. shows the elastic properties of steel bars and metal mesh.

Tenax mesh was modeled as biaxial Lumina material which has equivalent stress in both main directions (transverse and longitudinal directions) and also has the same fail stress in both directions.so it has isotropic and linear behavior only. Mesh thickness was 2.4 mm and modulus of elasticity (161.5 Mpa) and tensile density strength (94 N/mm2) at MD and (69.44 N/mm2) at TD.

Steel bars, metal meshes and tenax were modeled as embedded region in the surrounding solid elements in the concrete box girder as shown in Fig. (20).

The loads were modeled as pressure on contact area which was (90× 500 mm) for every load. The bottom surface of concrete box girder was prevented from translation YZ directions and from rotation about XZ direction at the two lines of contact with underneath roller supports. Concrete box girder was exposed to two concentrated loads at equivalent distance from supports line. Loads and boundary conditions were illustrated in Fig. (21).

The models were divided into fine elements with different sizes to allow quick analysis with sufficient accuracy. Total number of elements reached (374212) with sides varied from (12.5×12.5×12.5) mm to (25 × 25 ×25) mm. The fine element size was concentrated in region between applied loads in the middle of girder as shown in Fig. (22) while the coarse fine was provided near girder supports.

TABLE VII. ELASTIC PROPERTIES OF CONCRETE.

Parameter	**Value**
Density	2.4×10^{-9} N/mm3
Modulus oMod of elasticity (Es)	21900 MPa
Poisson's ratio (υ)	0.168

TABLE VIII. CONCRETE PLASTICITY PARAMETERS.

Parameter	**Value**
Dilation angle	42^{o}
Eccentricity	0.11
fb_0/fc_0	1.35
K	0.68
Viscosity parameter	0.0001
Yield stress in compression	17 MPa
Cross bonding inelastic strain	0.0
Compressive ultimate stress	33MPa
Cross bonding inelastic strain	0.00158
Tensile failure stress	3.45 MPa

TABLE IX.THE ELASTIC PROPERTIES OF STEEL BARS AND METAL MESHES.

Steel 24/35		**Steel 36/52**		**Expanded mesh**	
Density		**Density**		**Density**	
7.8×10^{-9}		7.8×10^{-9}		7.8×10^{-9}	
E	**Poissons ratio**	**E**	**Poissons ratio**	**E**	**Poissons ratio**
200000	0.3	130000	0.28	130000	0.28
stress	**strain**	**stress**	**strain**	**stress**	**strain**
235.35	0	199	0.00	199	0.00
353.03	0.0951	320	4.95E-02	320	4.95E-02

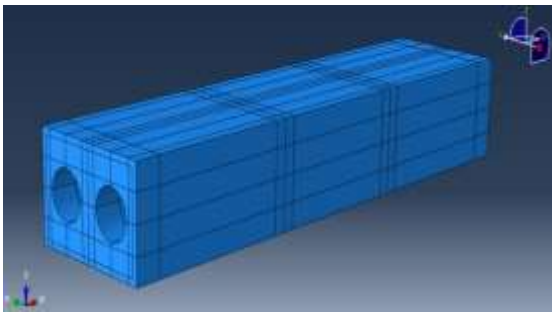

a) modeling of concrete box girder

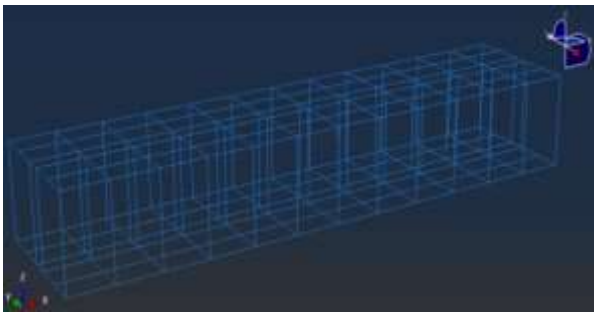

b) modeling of Steel bars and stirrups

Proc. Of the 5th International E-Conference on Advances in Engineering, Technology and Management - ICETM 2021

ISBN: 978-1-63248-192-4 DOI: 10.15224/ 978-1-63248-192-4-13

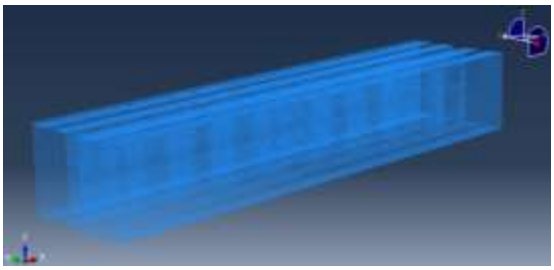

c) modeling of channels

d) modeling of circular mesh

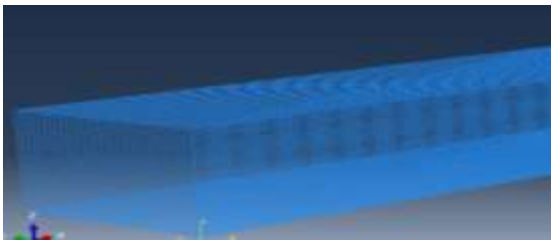

e) modeling of welded metal mesh

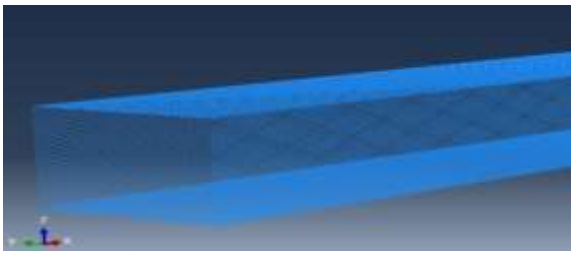

f) modeling of Expanded metal mesh

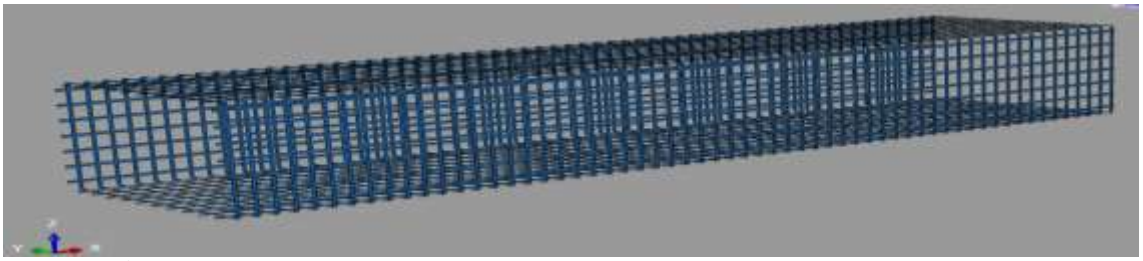

g) modeling of Tenax mesh

Figure 19. Modeling of model parts.

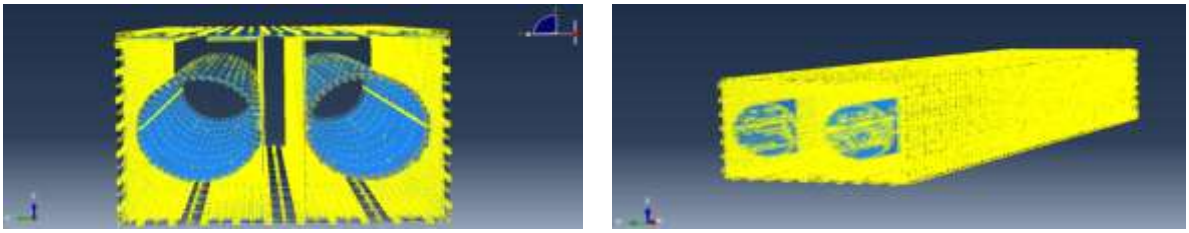

Figure 20. Interaction.

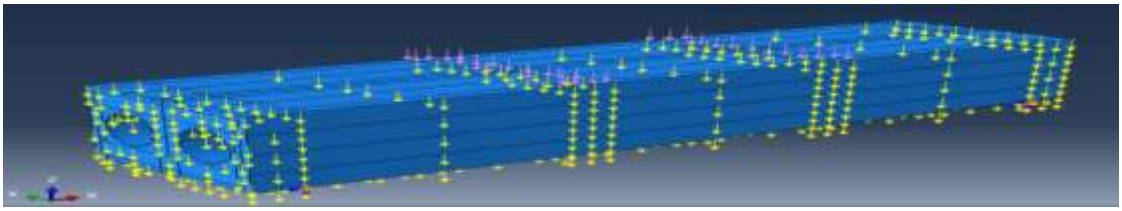

Figure 21. Boundary condition of model and loads.

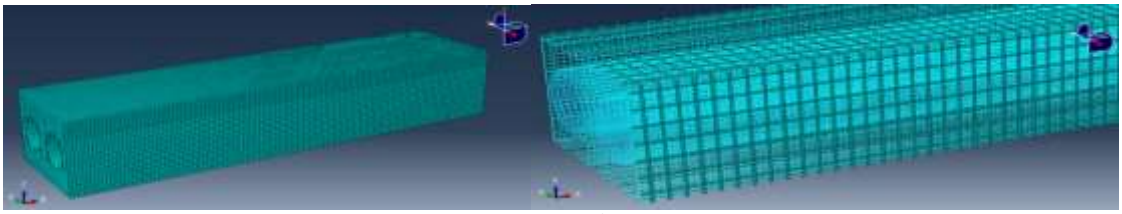

Figure 22. Meshing of model parts.

Proc. Of the 5th International E-Conference on Advances in Engineering, Technology and Management - ICETM 2021

ISBN: 978-1-63248-192-4 DOI: 10.15224/ 978-1-63248-192-4-13

B. *Comparison between Experimental and Finite Element Simulation Results*

The comparison between experimental and FE simulation results ultimate load, 1st crack load, mid span deflection at the ultimate load are illustrated in Table X. Fig. (23) and Fig. (24) present the applied load-mid span deflection, and the applied load-strain curves; respectively as obtained from the experimental and theoretical results for the all tested girders. The first crack load was determined as the first deviation from linearity of load deflection curve. The comparison between the experimental and theoretical cracking patterns for all tested specimens is presented in Fig. (25). Stresses distribution for all tested girders can be obtained at Fig. (26). Consequently, it can be concluded that the FE simulations give accurate results in comparing with the experimental results.

In addition, these comparisons indicate a good agreement in slope of curves in the linear stage. For nonlinear stage, and due to the possibility of the inaccuracy in modeling the post yield behaviour of steel rebar material, there is somewhat none agreement between the finite element results and those of experimental results**.**

TABLE X. A COMPARISON BETWEEN THE EXPERIMENTAL AND THEORETICAL RESULTS.

Specimens Designation	Specimen No.	First Crack load (KN)			Ultimate Load (KN)			Maximum deflection (mm)		
		Finite element method results	Experimental study results	Percentage of difference	Finite element method results	Experimental study results	Percentage of difference	Finite element method results	Experimental study results	Percentage of difference
1	B1	167.42	156.3	1.07	478.3	480	.996	41.4	41	1.009
	B2	179.42	165.6	1.083	512.6	480.7	1.066	47.7	51.9	.919
2	B3	170.52	160.5	1.062	532.8	523.6	1.017	25	25.78	.9697
	B4	172.36	162.3	1.062	538.7	525	1.025	20.8	21.23	.979
	B5	174.11	165.3	1.053	544.1	531.1	1.024	20.4	19.35	1.054
3	B6	166.52	157.5	1.057	520.4	522	.996	17.7	16.58	1.05
	B7	179.66	167.3	1.074	560.3	542.5	1.032	9.838	10.94	.899
4	B8	174.24	158.5	1.099	436.6	420.7	1.037	29.66	32.3	.918
	B9	172.96	160.3	1.079	494.2	482	1.025	41	43.03	.953

Proc. Of the 5th International E-Conference on Advances in Engineering, Technology and Management - ICETM 2021

ISBN: 978-1-63248-192-4 DOI: 10.15224/ 978-1-63248-192-4-13

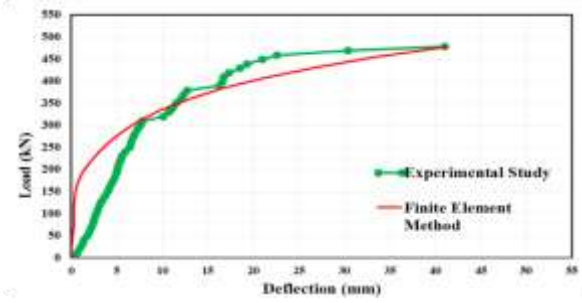

a) load-deflection curves for girder B1

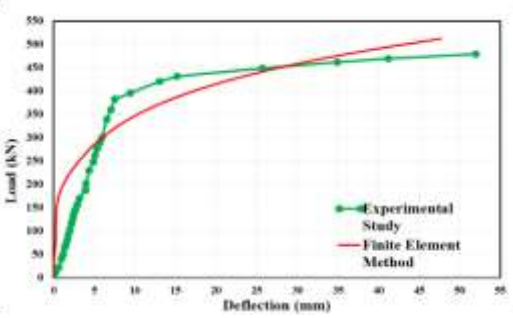

b) load-deflection curves for girder B2

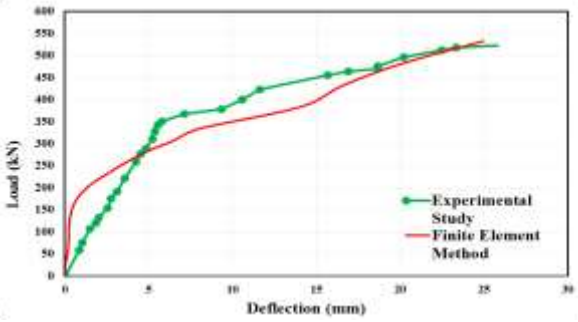

c) load-deflection curves for girder B3

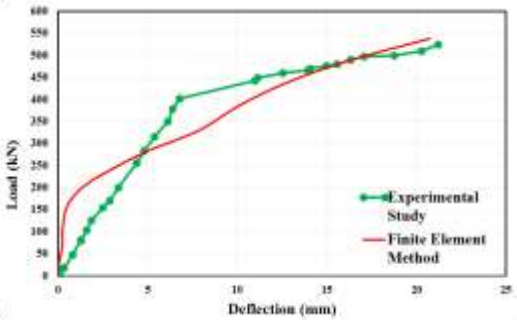

d) load-deflection curves for girder B4

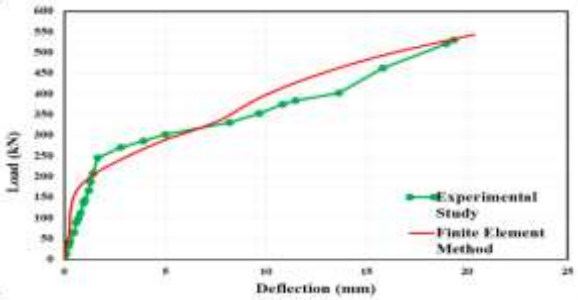

e) load-deflection curves for girder B5

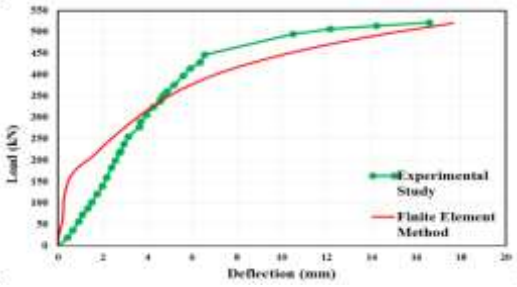

f) load-deflection curves for girder B6

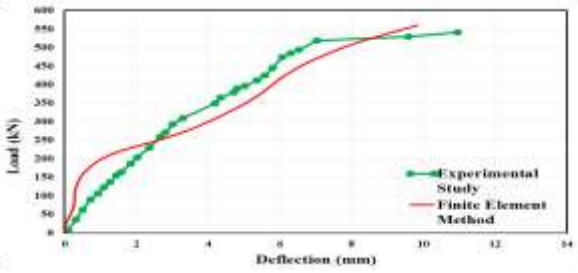

g) load-deflection curves for girder B7

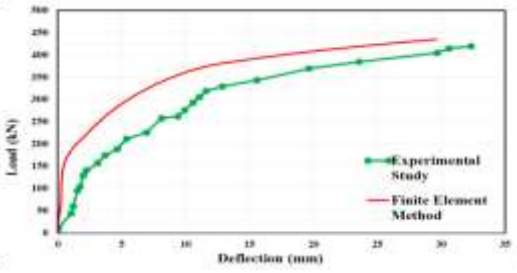

h) load-deflection curves for girder B8

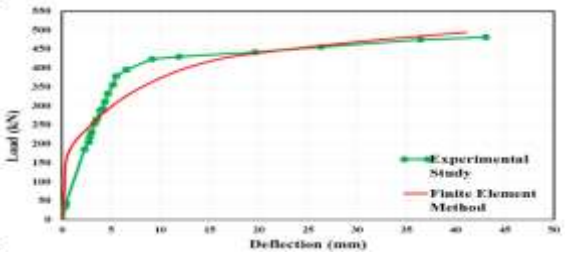

K) load-deflection curves for girder B9

Figure 23. Load-deflection curve for test specimens for experimental and theoretical results.

Proc. Of the 5th International E-Conference on Advances in Engineering, Technology and Management - ICETM 2021

ISBN: 978-1-63248-192-4 DOI: 10.15224/ 978-1-63248-192-4-13

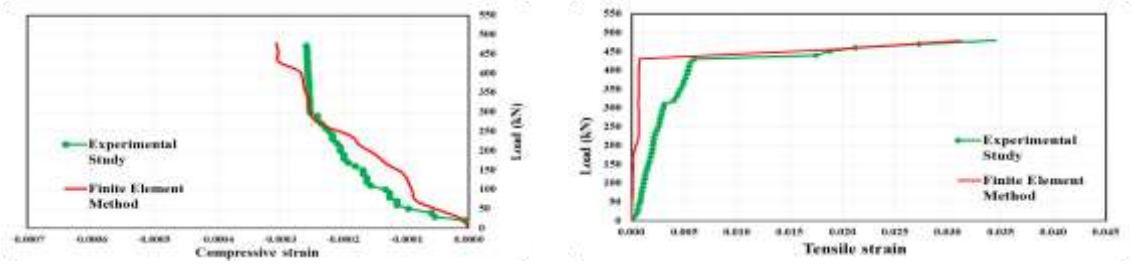

a) Load- strain curves of girder B1

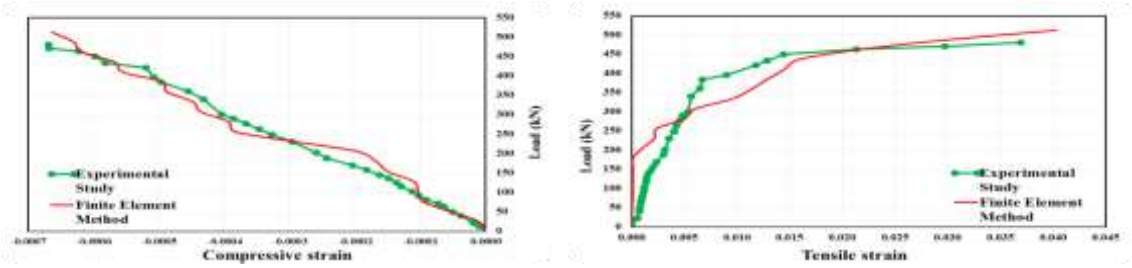

b) Load- strain curves of girder B2

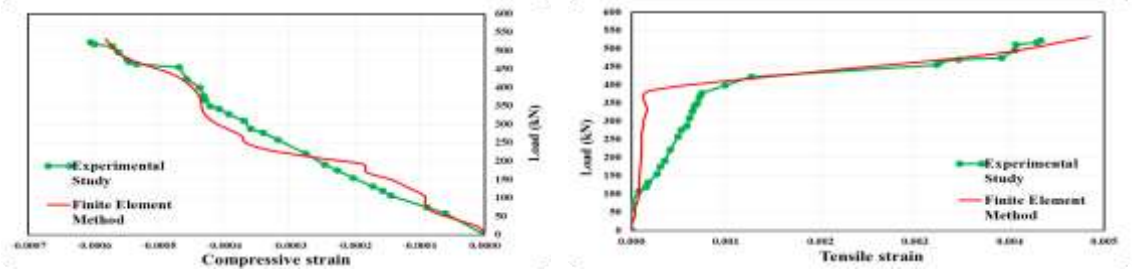

c) Load- strain curves of girder B3

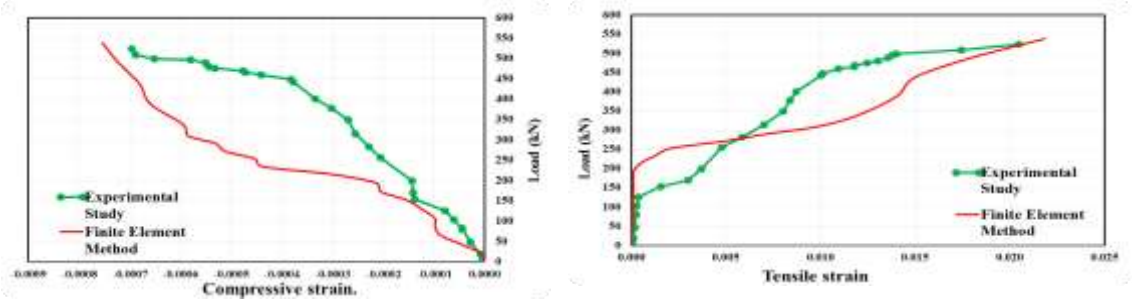

d) Load- strain curves of girder B4

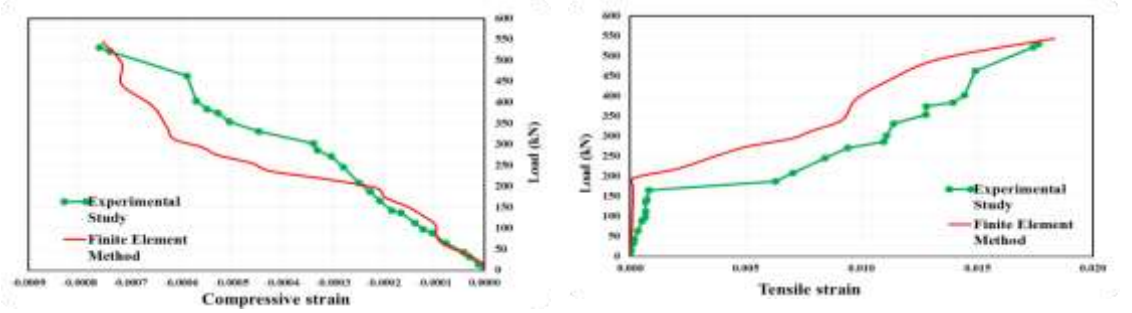

e)Load- strain curves of girder B5

Proc. Of the 5th International E-Conference on Advances in Engineering, Technology and Management - ICETM 2021

ISBN: 978-1-63248-192-4 DOI: 10.15224/ 978-1-63248-192-4-13

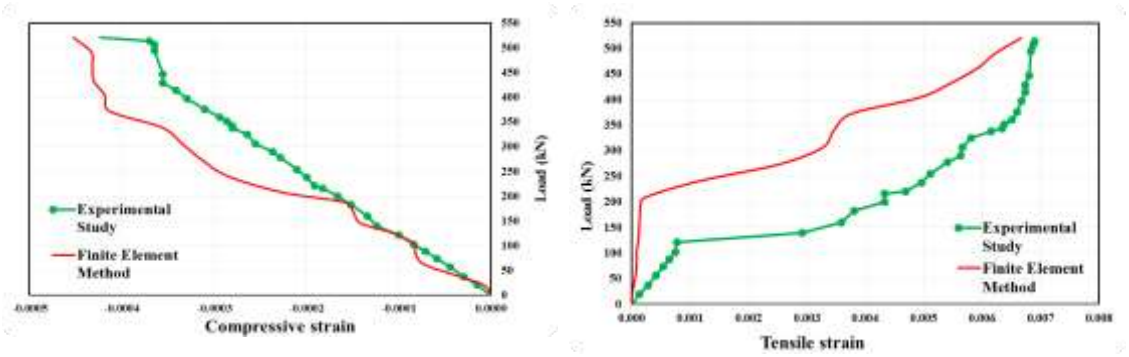

f) Load- strain curves of girder B6

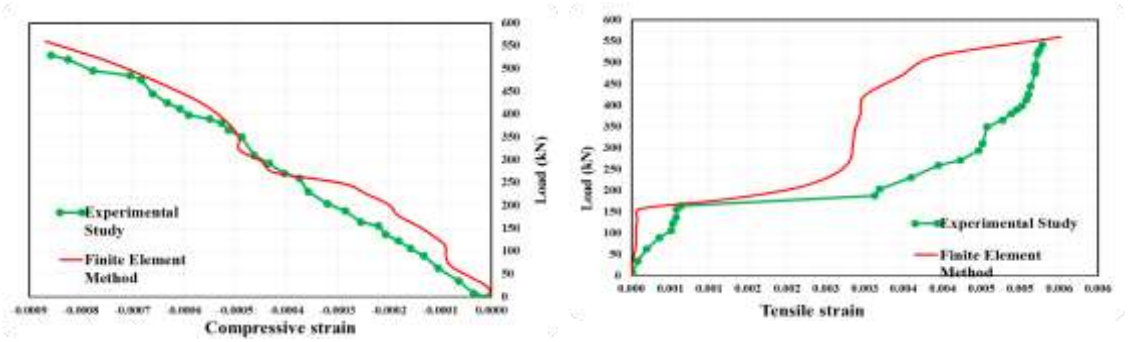

g) Load- strain curves of girder B7

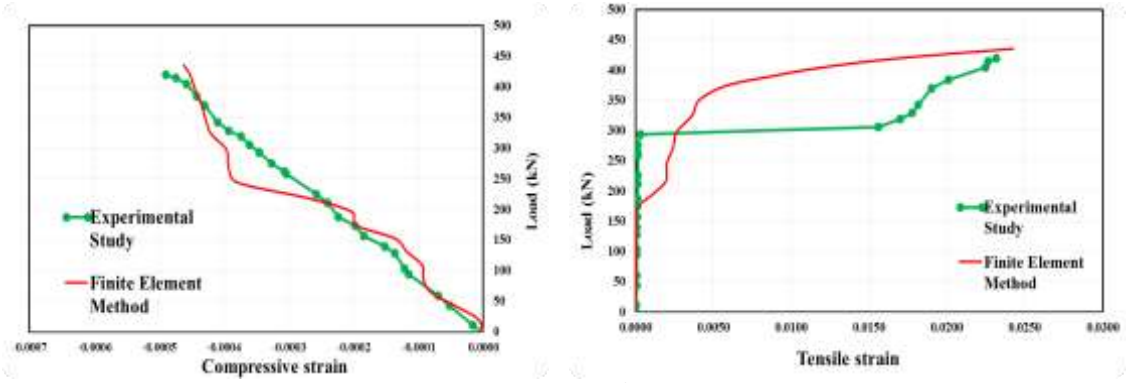

h) Load- strain curves of girder B8

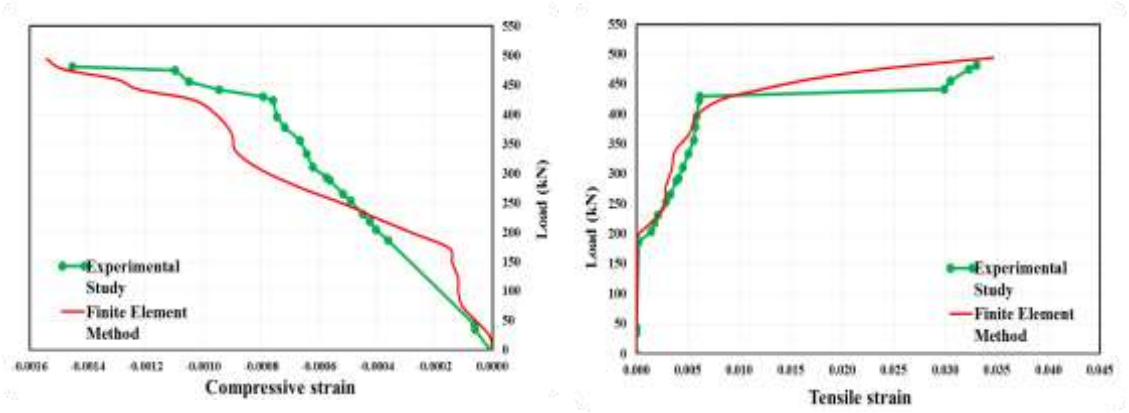

k) Load- strain curve of girder B9

Figure 24. Load- strain curves for tested girders for experimental and theoretical results.

Proc. Of the 5th International E-Conference on Advances in Engineering, Technology and Management - ICETM 2021

ISBN: 978-1-63248-192-4 DOI: 10.15224/ 978-1-63248-192-4-13

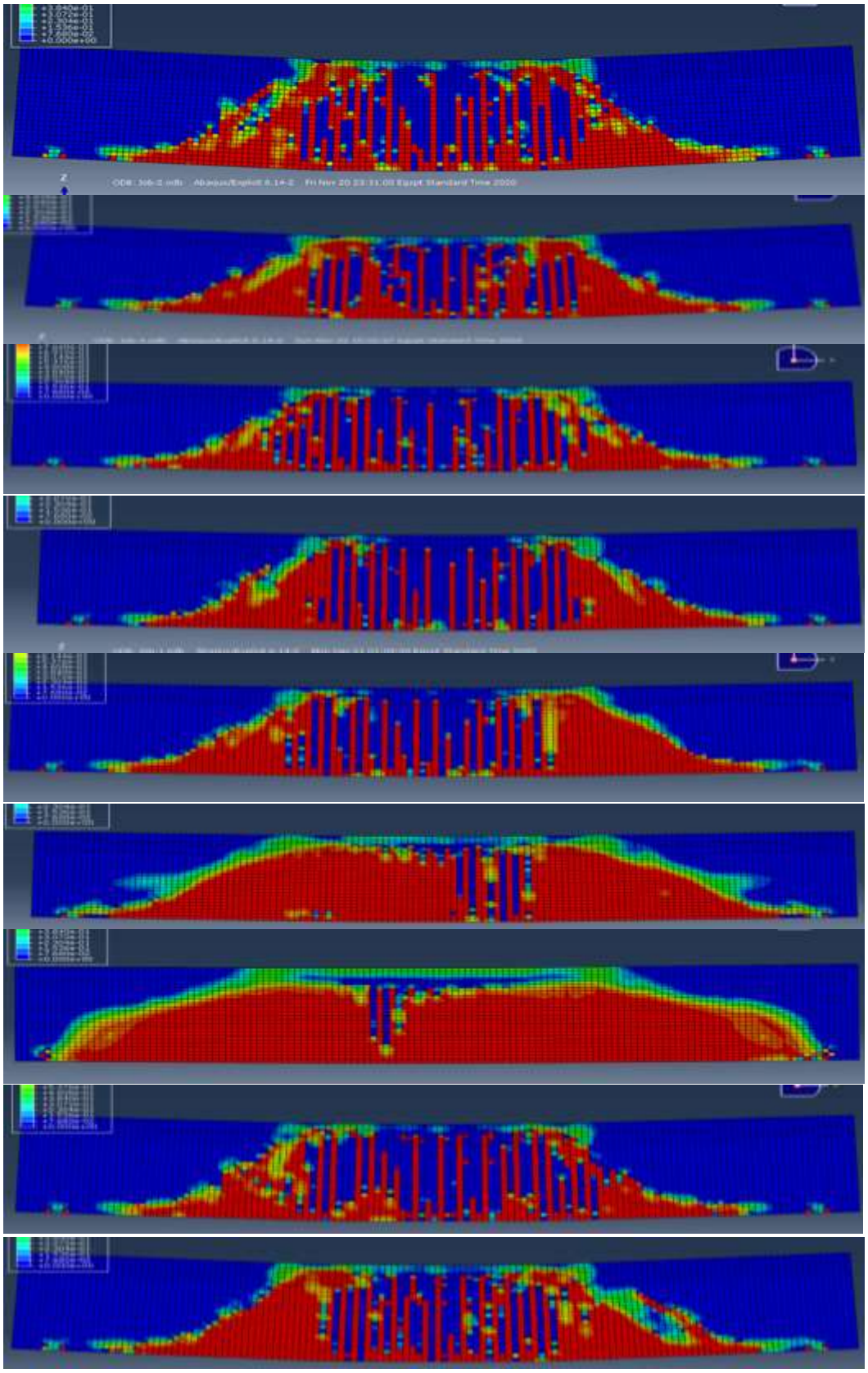

Figure 25. Cracking patterns for all tested girders from the theoretical study.

ISBN: 978-1-63248-192-4 DOI: 10.15224/ 978-1-63248-192-4-13

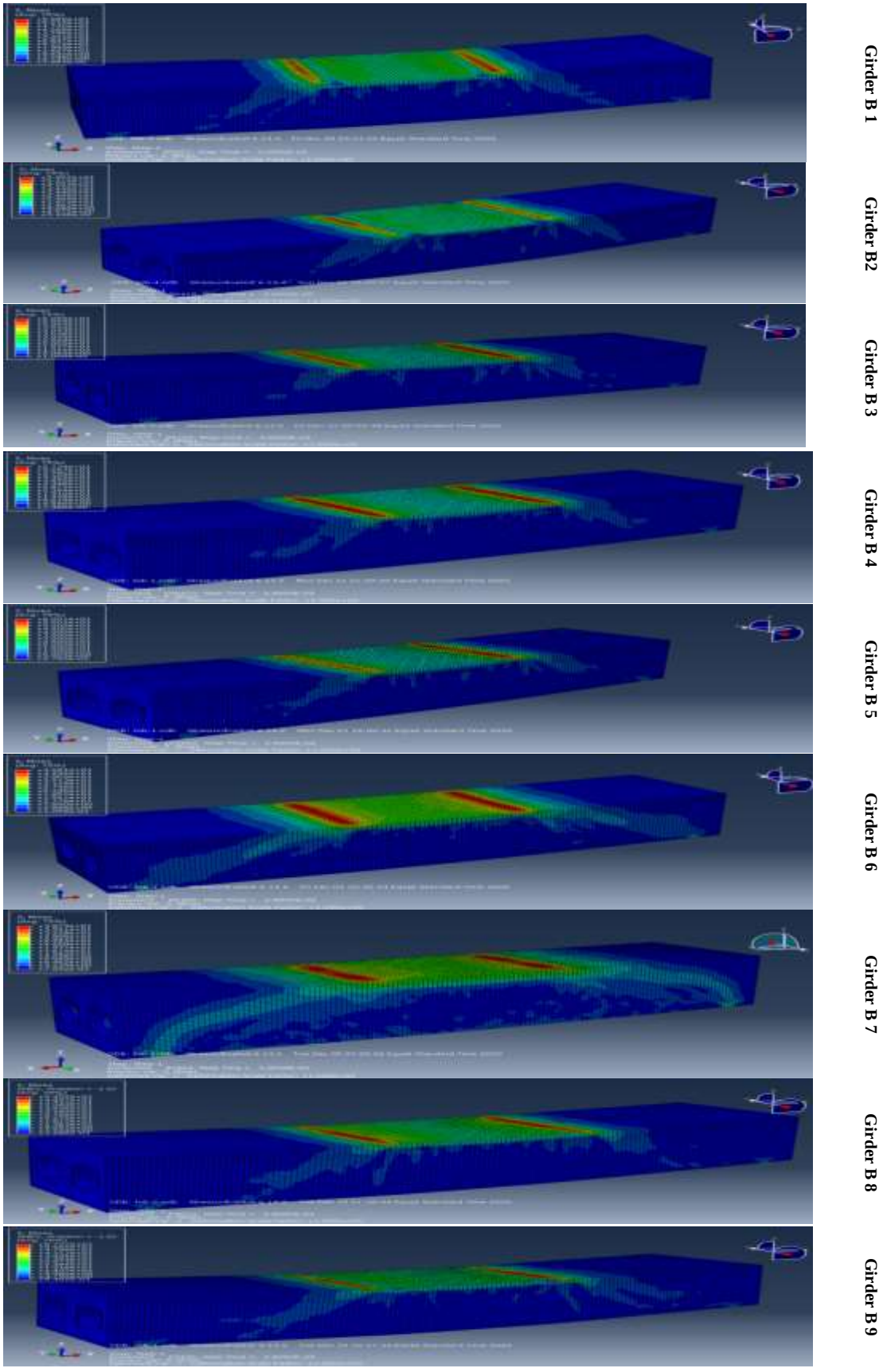

Figure 26. Stress distribution for all tested girders from the theoretical study.

ISBN: 978-1-63248-192-4 DOI: 10.15224/ 978-1-63248-192-4-13

IV. Conclusions

Based on the experimentally-available results and the FE numerical study conducted, the following conclusions are drawn:

1- Using two layers of expanded metal mesh in reinforcing ferrocement girders clearly increased the ultimate moment, decrease deflection, and improve the energy absorption than using other types of meshes.

2- Using two layers of welded steel mesh increased the ultimate load by percentage (9.4%) and decrease maximum deflection at mid span by percentage (39%) from control girder.

3- Using three layers of welded steel mesh increased the ultimate load by percentage (12.64 %) and decrease maximum deflection at mid span by percentage (50%) from control girder.

4- Using four layers of welded steel mesh increased the ultimate load by percentage (13.77%) and decrease maximum deflection at mid span by percentage (53%) from control girder.

5- Using one layer of expanded steel mesh increased the ultimate load by percentage (9%) and decrease maximum deflection at mid span by percentage (57%) from control girder.

6-Using two layers of expanded steel mesh increased the ultimate load by percentage (17.17%) and decrease maximum deflection at mid span by percentage (76%) from control girder.

7-In general**, while** the developed ferrocement box girder emphasized better deformation characteristics and high serviceability loads, crack resistance, it led to a decrease of ductility.

8- The best behavior of box girder was that of using double layers of expanded metal mesh as additional reinforcement with main steel.

9- There is a great saving of weight by making voids area in the cross section leading to easy construction especially for weak soil foundations.

10- A numerical FE model based on the finite element theory can be used to investigate the flexural behavior of ferrocement girders reinforced with composite material, leading to a good agreement when comparing to available full-scale test data.

11- Increasing the number of the steel mesh layers in the ferrocement forms increases the first crack load, service load, ultimate load, and energy absorption decreases the ductility ratio of the girders.

V. References

[1] ACI 549R-97 (2009), State-of-the-Art Report on Ferrocement, American Concrete Institute, Detroit, MI 48219, USA.

[2] Shaheen, Y. B., & Eltehawy, E. A. (2017). Structural behaviour of ferrocement channels slabs for low cost housing. Challenge J. Concr. Res. Lett, 8(2), 48-64.

[3] Abdul-Fataha, S. (2014). Structural behavior of concrete beams reinforced with innovative materials (Doctoral dissertation, M. Sc. thesis, Minufiya University, Shebin El-Kom, Egypt).

[4] Shaheen, Y., Eltaly, B. and Abdul-Fataha, S. (2014), "Structural performance of ferrocement beams reinforced with composite materials", Struct. Eng. Mech., 50(6), 817-834.

[5] Singh, V., Bansal, P. P., & Kumar, M. (2015). Experimental studies on strength and ductility of ferrocement jacketed RC beam-column joints. International Journal of Civil and Structural Engineering, 5(3), 199-205.

[6] Ramakrishnan, K., Muthu, D., & Viveka, S. (2020). An Experimental Investigation of Flexural Behaviour of Ferrocement Box Beams Using Micro Fillers. In Sustainable Practices and Innovations in Civil Engineering (pp. 87-96).

[7] Acma, L. M. C., Dumpasan, G. C., Salva, M. L. I., Mansaguiton, M. P., Supremo, R. P., & Daquiado, N. F. P. (2015). Flexural strength and ductility behavior of ferrocement I-beam. Mindanao Journal of Science and Technology, 13.

[8] Eskandari, H., & Madadi, A. (2015). Investigation of ferrocement channels using experimental and finite element analysis. Engineering Science and Technology, an International Journal, 18(4), 769-775.

[9] Dajun, D., July (1993) "Ferrocement Structures in China," Journal of ferrocement, Vol. 23, No. 3, PP. 213-224.

[10] Abbass, A. A., Abid, S. R., Arna'ot, F. H., Al-Ameri, R. A., & Özakça, M. (2020, February). Flexural response of hollow high strength concrete beams considering different size reductions. In Structures (Vol. 23, pp. 69-86).

[11] Du, W., Yang, C., Wang, C., Pan, Y., Zhang, H., & Yuan, W. (2021). Flexural Behavior of Polyvinyl Alcohol Fiber–Reinforced Ferrocement Cementitious Composite. Journal of Materials in Civil Engineering, 33(4), 04021040.

[12] Naser, F. H., Al Mamoori, A. H. N., & Dhahir, M. K. (2020). Effect of using different types of reinforcement on the flexural behavior of ferrocement hollow core slabs embedding PVC pipes. Ain Shams Engineering Journal.

[13] Egyptian Standards Specification, E.S.S, 4756-11. (2012). Physical and mechanical properties examination of cement, part 1, Cairo.

[14] E.C.P.203/2007. Egyptian Code of Practice: Design and Construction for Reinforced Concrete Structures. Cairo, Egypt, 2007.

[15] ASTM C1116/C1116M—10a. (2015). Standard specification for fiber reinforced concrete. ASTM international, West Conshohocken, PA. http://www.astm.org/.

[17] ASTM C618-19.(2019) , Standard Specification for Coal Fly Ash and Raw or Calcined Natural Pozzolan for Use in Concrete, ASTM International, West Conshohocken, PA,

[18] E.S.S.1109/2008. Aggregates for Concrete. Ministry of Industry, Cairo, Egypt, 2008